Chapter 7

Second-Order Statistics: Strong Fluctuation Theory

Overview: In Chap. 6 we introduced the *mutual coherence function* (MCF) based on weak fluctuation theory, whereas in this chapter we will examine the MCF based on methods applicable to strong fluctuation theory. Although several techniques have been used over the years to deal with the MCF under strong fluctuations, it has been shown that all of them are essentially equivalent to one another under certain assumptions. For that reason we limit our treatment of strong fluctuation theories to the *parabolic equation method* and the *extended Huygens-Fresnel principle.*

Of the above two methods, the one most similar to the Rytov approximation is the extended Huygens-Fresnel principle. Because it is somewhat easier to use than other methods, we will develop this technique in more detail than the parabolic equation method. In addition to these methods, we also introduce a more "heuristic approach" that uses the notion of "effective beam parameters" to redefine the free-space Gaussian beam in terms of

an effective Gaussian-beam wave that takes into account the refractive and diffractive characteristics imposed on the beam by the random medium. The method of effective beam parameters is used to develop an expression for the spatial coherence radius of a Gaussian-beam wave and to extend the beam wander variance developed in Chap. 6 to conditions of moderate-to-strong irradiance fluctuations.

7.1 Introduction

We used the *Rytov approximation* in Chap. 6 to produce a number of useful results for second-order statistics under weak irradiance fluctuations. For more general turbulence conditions, other methods must be employed like the parabolic equation method [1,2], extended Huygens-Fresnel principle [3,4], or Feynman path integral [5,6]. For a beam propagating over a path of length L, we can distinguish between *weak fluctuation conditions* and *strong fluctuation conditions* by imposing requirements on the Rytov variance $\sigma_R^2 = 1.23C_n^2k^{7/6}L^{11/6}$ or on the parameter $q = L/k\rho_{\text{pl}}^2$, where k is the optical wave number, C_n^2 is the refractive index structure constant, and ρ_{pl} is the spatial coherence radius of a plane wave. In particular, for a Kolmogorov power-law spectrum, the Rytov variance criterion leads to the sets of inequalities (Section 5.2):

$$\begin{aligned} &\sigma_R^2 < 1 \quad \text{and} \quad \sigma_R^2\Lambda^{5/6} < 1, \quad \text{(weak fluctuation conditions)},\\ &\sigma_R^2 \gg 1 \quad \text{or} \quad \sigma_R^2\Lambda^{5/6} \gg 1, \quad \text{(strong fluctuation conditions)}, \end{aligned} \tag{1}$$

where $\Lambda = 2L/kW^2$ is the Gaussian beam parameter characterizing the spot size W at the receiver. For an arbitrary spectral model, the corresponding expressions in terms of the more general parameter q are given by the following sets of inequalities:

$$\begin{aligned} &q < 1 \quad \text{and} \quad q\Lambda < 1, \quad \text{(weak fluctuation conditions)},\\ &q \gg 1 \quad \text{or} \quad q\Lambda \gg 1, \quad \text{(strong fluctuation conditions)}. \end{aligned} \tag{2}$$

Most of the methods of analysis proposed above (and others) for dealing with strong fluctuation conditions were reviewed by Strohbehn [7] and by Yura [8] and shown that, up to second-order moments of the field, these methods are equivalent to each other under appropriate restrictions. Thus, for the purpose of calculating the first-order and second-order field moments, we will rely here primarily on the extended Huygens-Fresnel principle and the parabolic equation method, both briefly discussed in Section 5.8. Unfortunately, only asymptotic results have been obtained thus far by any of these methods for the fourth-order field moment (see Chaps. 8 and 9). Moreover, it has not been established that all these methods are equivalent for the fourth-order field moments. It has been widely accepted, however, that the parabolic equations developed for the higher-order field moments are more fundamental than formulations by other methods under strong irradiance fluctuations.

7.2 Parabolic Equation Method

In Section 5.8.1 we briefly introduced the *parabolic equation method.* This method is based on establishing parabolic equations for each of the field moments like the mean field, mutual coherence function, and the fourth-order coherence function. The starting point for the formulation of these moments is the *parabolic equation*

$$2ik\frac{\partial V(\mathbf{R})}{\partial z} + \nabla_T^2 V(\mathbf{R}) + 2k^2 n_1(\mathbf{R})V(\mathbf{R}) = 0, \tag{3}$$

deduced from the stochastic Helmholtz equation by making the substitution $U(\mathbf{R}) = V(\mathbf{R})e^{ikz}$ and using the simplifying assumptions given by Eqs. (8) in Chap. 4 for deriving the paraxial equation. Here, k is the optical wave number, $\mathbf{R} = (\mathbf{r}, z)$ is a point in space, $n_1(\mathbf{R})$ is the random index of refraction with zero mean, and $\nabla_T^2 = \partial^2/\partial x^2 + \partial^2/\partial y^2$ is transverse Laplacian operator.

7.2.1 Mean field

The term-by-term ensemble average of Eq. (3) produces a differential equation for the mean field $\langle V(\mathbf{R})\rangle$ given by

$$2ik\frac{\partial}{\partial z}\langle V(\mathbf{R})\rangle + \nabla_T^2\langle V(\mathbf{R})\rangle + 2k^2\langle n_1(\mathbf{R})V(\mathbf{R})\rangle = 0. \tag{4}$$

Here now we see the mathematical difficulty associated with this approach—namely, the last term on the left introduces another unknown $\langle n_1(\mathbf{R})V(\mathbf{R})\rangle$ into the equation. Tatarskii and Klyatskin [9] found a way around this dilemma by using the notion that the refractive index is uncorrelated (i.e., delta correlated) in the direction of propagation. This approximation, which involves the notion of functional derivative and the Furutsu-Novikov formula [10,11], leads to the result

$$\langle n_1(\mathbf{R})V(\mathbf{R})\rangle = \frac{ik}{2}A_n(0)\langle V(\mathbf{r}, z)\rangle, \tag{5}$$

where $A_n(0)$ for a statistically homogeneous and isotropic medium is defined by (see Section 5.2.1)

$$A_n(0) = 4\pi^2\int_0^\infty \kappa\Phi_n(\kappa)\,d\kappa. \tag{6}$$

Therefore, Eq. (4) becomes

$$\left[2ik\frac{\partial}{\partial z} + \nabla_T^2 + ik^3A_n(0)\right]\langle V(\mathbf{r}, z)\rangle = 0. \tag{7}$$

If we also prescribe the boundary condition at the input plane ($z = 0$)

$$\langle V(\mathbf{r}, 0)\rangle = V_0(\mathbf{r}, 0) = U_0(\mathbf{r}, 0), \tag{8}$$

the resulting boundary value problem consisting of (7) and (8) completely describes the *coherent field* $\langle V(\mathbf{r}, z)\rangle$.

To solve (7), we look for a solution of the form

$$\begin{aligned}\langle V(\mathbf{r}, z)\rangle &= w(\mathbf{r}, z)\exp\left[-\frac{1}{2}k^2 z A_n(0)\right] \\ &= w(\mathbf{r}, z)\exp\left[-2\pi^2 k^2 z\int_0^\infty \kappa\Phi_n(\kappa)\,d\kappa\right],\end{aligned} \tag{9}$$

where $w(\mathbf{r}, z)$ is an unknown function. The direct substitution of (9) into (7) leads to

$$\left[2ik\frac{\partial}{\partial z} + \nabla_T^2\right]w(\mathbf{r}, z) = 0. \tag{10}$$

However, we recognize (10) as the parabolic equation for the field in free space [recall Eq. (9) in Chap. 4] so that we can identify the function $w(\mathbf{r}, z)$ as the free-space field at the output plane, viz., $w(\mathbf{r}, z) = V_0(\mathbf{r}, z)$. Consequently, by writing $V(\mathbf{r}, z) = U(\mathbf{r}, z)e^{-ikz}$, we obtain for the *mean field*

$$\langle U(\mathbf{r}, z)\rangle = U_0(\mathbf{r}, z)\exp\left[-2\pi^2 k^2 z\int_0^\infty \kappa\Phi_n(\kappa)\,d\kappa\right], \tag{11}$$

which is the same result as that given by Eq. (27) in Chap. 6 using the Rytov approximation.

7.2.2 Mutual coherence function

The second-order field moment

$$\Gamma_2(\mathbf{r}_1, \mathbf{r}_2, z) = \langle U(\mathbf{r}_1, z)U^*(\mathbf{r}_2, z)\rangle = \langle V(\mathbf{r}_1, z)V^*(\mathbf{r}_2, z)\rangle, \tag{12}$$

where $\mathbf{r}_1$ and $\mathbf{r}_2$ denote two points in the transverse plane at propagation distance z, is called the *mutual coherence function* (MCF). To obtain the governing differential equation for this quantity, we start with the parabolic equation (3) expressed as

$$2ik\frac{\partial V(\mathbf{r}_1, z)}{\partial z} + \nabla_{T1}^2 V(\mathbf{r}_1, z) + 2k^2 n_1(\mathbf{r}_1, z)V(\mathbf{r}_1, z) = 0, \tag{13}$$

and multiply it by $V^*(\mathbf{r}_2, z)$ to obtain

$$\begin{aligned}2ik\frac{\partial V(\mathbf{r}_1, z)}{\partial z}V^*(\mathbf{r}_2, z) &+ \nabla_{T1}^2 V(\mathbf{r}_1, z)V^*(\mathbf{r}_2, z) \\ &+ 2k^2 n_1(\mathbf{r}_1, z)V(\mathbf{r}_1, z)V^*(\mathbf{r}_2, z) = 0,\end{aligned} \tag{14}$$

where ∇_{T1}^2 is the transverse Laplacian with respect to $\mathbf{r}_1$. If we now take the complex conjugate of (13), interchange the roles of $\mathbf{r}_1$ and $\mathbf{r}_2$, and multiply by $V(\mathbf{r}_1, z)$, we get

$$-2ik\frac{\partial V^*(\mathbf{r}_2,z)}{\partial z}V(\mathbf{r}_1,z)+\nabla_{T2}^2V(\mathbf{r}_1,z)V^*(\mathbf{r}_2,z)$$
$$+2k^2n_1(\mathbf{r}_1,z)\times V(\mathbf{r}_1,z)V^*(\mathbf{r}_2,z)=0. \tag{15}$$

Subtracting (15) from (14), followed by taking the ensemble average of the resulting expression, then leads to the differential equation

$$2ik\frac{\partial}{\partial z}\Gamma_2(\mathbf{r}_1,\mathbf{r}_2,z)+\left(\nabla_{T1}^2-\nabla_{T2}^2\right)\Gamma_2(\mathbf{r}_1,\mathbf{r}_2,z)$$
$$+2k^2\langle[n_1(\mathbf{r}_1,z)-n_1(\mathbf{r}_2,z)]V(\mathbf{r}_1,z)V^*(\mathbf{r}_2,z)\rangle=0. \tag{16}$$

Once again we need to resolve the last term on the left in (16). Based on the Furutsu-Novikov formula, it has been shown that [2]

$$\begin{aligned}\langle n_1(\mathbf{r}_1,z)V(\mathbf{r}_1,z)V^*(\mathbf{r}_2,z)\rangle&=\frac{ik}{2}[A_n(0)-A_n(\mathbf{r}_1-\mathbf{r}_2)]\Gamma_2(\mathbf{r}_1,\mathbf{r}_2,z),\\ \langle n_1(\mathbf{r}_2,z)V(\mathbf{r}_1,z)V^*(\mathbf{r}_2,z)\rangle&=-\frac{ik}{2}[A_n(0)-A_n(\mathbf{r}_1-\mathbf{r}_2)]\Gamma_2(\mathbf{r}_1,\mathbf{r}_2,z),\end{aligned} \tag{17}$$

and, thus, Eq. (16) becomes

$$2ik\frac{\partial}{\partial z}\Gamma_2(\mathbf{r}_1,\mathbf{r}_2,z)+\left(\nabla_{T1}^2-\nabla_{T2}^2\right)\Gamma_2(\mathbf{r}_1,\mathbf{r}_2,z)$$
$$+2ik^3[A_n(0)-A_n(\mathbf{r}_1-\mathbf{r}_2)]\Gamma_2(\mathbf{r}_1,\mathbf{r}_2,z)=0. \tag{18}$$

The form of the boundary condition for the MCF at the input plane ($z=0$) depends on the nature of the transmitted optical wave. In the case of an infinite plane wave, for example, the boundary condition is simply

$$\Gamma_2(\mathbf{r}_1,\mathbf{r}_2,0)=1. \tag{19}$$

Thus, the solution of (18) leads to

$$\begin{aligned}\Gamma_2(\mathbf{r}_1,\mathbf{r}_2,z)&=\exp\left\{-k^2z[A_n(0)-A_n(\mathbf{r}_1-\mathbf{r}_2)]\right\}\\ &=\exp\left\{-4\pi^2k^2z\int_0^\infty\kappa\Phi_n(\kappa)[1-J_0(\kappa\rho)]\,d\kappa\right\},\end{aligned} \tag{20}$$

where we have assumed isotropy and used Eq. (11) in Chap. 5. We recognize this last expression as the same result given by Eq. (48) in Chap. 6 that was previously derived by using the Rytov approximation. Hence, the MCF for a plane wave is the same in both weak and strong fluctuation regimes. The same holds true for a spherical wave, but this is not the case for a Gaussian-beam wave as shown below in Section 7.3. That is, the expression developed in Section 6.3.3 is not valid under strong fluctuations.

7.3 Extended Huygens-Fresnel Principle

If $U_0(\mathbf{r}, 0)$ denotes the optical wave field at the transmitter, the field of the wave after propagating a distance L through a random medium is defined by the *extended Huygens-Fresnel principle* [3,4]

$$U(\mathbf{r}, L) = -\frac{ik}{2\pi L}\exp(ikL)\int\int_{-\infty}^{\infty} d^2 s U_0(\mathbf{s}, 0)\exp\left[\frac{ik|\mathbf{s}-\mathbf{r}|^2}{2L} + \psi(\mathbf{r}, \mathbf{s})\right], \tag{21}$$

where $\psi(\mathbf{r}, \mathbf{s}) = \psi_1(\mathbf{r}, \mathbf{s}) + \psi_2(\mathbf{r}, \mathbf{s})$ is the random part of the complex phase of a spherical wave propagating in the turbulent medium from the point $(\mathbf{s}, 0)$ to the point $(\mathbf{r}, L)$. As with the Rytov method, we assume both first-order and second-order perturbations.

7.3.1 Second-order moments of the complex phase perturbation

Comparable to that in Chap. 6, we find that the statistical quantities of interest derived from Eq. (21) can all be formulated in terms of three second-order moments associated with the complex phase perturbations. In the present case, if the random medium is *statistically homogeneous* and *isotropic*, these moments are given by [12]

$$\begin{aligned} E_1(0,0;0,0) &= \langle \psi_2(\mathbf{r}, \mathbf{s})\rangle + \frac{1}{2}\langle \psi_1^2(\mathbf{r}, \mathbf{s})\rangle \\ &= -2\pi^2 k^2 L\int_0^{\infty} \kappa\Phi_n(\kappa)\, d\kappa, \end{aligned} \tag{22}$$

$$\begin{aligned} E_2(\mathbf{r}_1, \mathbf{r}_2; \mathbf{s}_1, \mathbf{s}_2) &= \langle \psi_1(\mathbf{r}_1, \mathbf{s}_1)\psi_1^*(\mathbf{r}_2, \mathbf{s}_2)\rangle \\ &= 4\pi^2 k^2 L\int_0^1\int_0^{\infty} \kappa\Phi_n(\kappa) J_0[\kappa|(1-\xi)\mathbf{p} + \xi\mathbf{Q}|]\, d\kappa\, d\xi, \end{aligned} \tag{23}$$

$$\begin{aligned} E_3(\mathbf{r}_1, \mathbf{r}_2; \mathbf{s}_1, \mathbf{s}_2) &= \langle \psi_1(\mathbf{r}_1, \mathbf{s}_1)\psi_1(\mathbf{r}_2, \mathbf{s}_2)\rangle \\ &= -4\pi^2 k^2 L\int_0^1\int_0^{\infty} \kappa\Phi_n(\kappa) J_0[\kappa|(1-\xi)\mathbf{p} + \xi\mathbf{Q}|] \\ &\quad \times \exp\left[-\frac{iL\kappa^2}{k}\xi(1-\xi)\right] d\kappa\, d\xi, \end{aligned} \tag{24}$$

where

$$\mathbf{p} = \mathbf{r}_1 - \mathbf{r}_2, \quad \mathbf{Q} = \mathbf{s}_1 - \mathbf{s}_2. \tag{25}$$

The zeros in the argument of E_1 indicate that this expression is independent of the location of the points $\mathbf{r}_1, \mathbf{r}_2$ and $\mathbf{s}_1, \mathbf{s}_2$.

We are most interested in the lower-order field moments deduced from the general formulation given by Eq. (21). This interest involves the *coherent portion* of the field or *mean field*

$$\langle U(\mathbf{r}, L)\rangle = -\frac{ik}{2\pi L}\exp(ikL)\int\int_{-\infty}^{\infty} d^2 s U_0(\mathbf{s}, 0)\exp\left[\frac{ik|\mathbf{s}-\mathbf{r}|^2}{2L}\right]\langle\exp[\psi(\mathbf{r}, \mathbf{s})]\rangle, \quad (26)$$

the general *second-order field moment* known as the MCF,

$$\begin{aligned}\Gamma_2(\mathbf{r}_1, \mathbf{r}_2, L) &= \langle U(\mathbf{r}_1, L)U^*(\mathbf{r}_2, L)\rangle \\ &= \left(\frac{k}{2\pi L}\right)^2\int\int\int\int_{-\infty}^{\infty} d^2 s_1 d^2 s_2 U_0(\mathbf{s}_1, 0)U_0^*(\mathbf{s}_2, 0)\exp\left[\frac{ik|\mathbf{s}_1-\mathbf{r}_1|^2}{2L}\right] \\ &\quad\times\exp\left[-\frac{ik|\mathbf{s}_2-\mathbf{r}_2|^2}{2L}\right]\langle\exp[\psi(\mathbf{r}_1, \mathbf{s}_1)+\psi^*(\mathbf{r}_2, \mathbf{s}_2)]\rangle, \end{aligned} \quad (27)$$

and the general *fourth-order moment* defined by

$$\begin{aligned}\Gamma_4(\mathbf{r}_1, \mathbf{r}_2, \mathbf{r}_3, \mathbf{r}_4, L) &= \langle U(\mathbf{r}_1, L)U^*(\mathbf{r}_2, L)U(\mathbf{r}_3, L)U^*(\mathbf{r}_4, L)\rangle \\ &= \left(\frac{k}{2\pi L}\right)^4\int\int\int\int\int\int\int\int_{-\infty}^{\infty} d^2 s_1 d^2 s_2 d^2 s_3 d^2 s_4 \\ &\quad\times U_0(\mathbf{s}_1, 0)U_0^*(\mathbf{s}_2, 0)U_0(\mathbf{s}_3, 0)U_0^*(\mathbf{s}_4, 0)\exp\left[\frac{ik|\mathbf{s}_1-\mathbf{r}_1|^2}{2L}\right] \\ &\quad\times\exp\left[-\frac{ik|\mathbf{s}_2-\mathbf{r}_2|^2}{2L}\right]\exp\left[\frac{ik|\mathbf{s}_3-\mathbf{r}_3|^2}{2L}\right]\exp\left[-\frac{ik|\mathbf{s}_4-\mathbf{r}_4|^2}{2L}\right] \\ &\quad\times\langle\exp[\psi(\mathbf{r}_1, \mathbf{s}_1)+\psi^*(\mathbf{r}_2, \mathbf{s}_2)+\psi(\mathbf{r}_3, \mathbf{s}_3)+\psi^*(\mathbf{r}_4, \mathbf{s}_4)]\rangle. \end{aligned} \quad (28)$$

In this chapter we examine only the first- and second-order moments (26) and (27), respectively. These first two moments are useful in predicting the additional beam spread of the optical wave caused by optical turbulence and also in predicting its subsequent loss of spatial coherence. The fourth-order moment (28), which we include only for the sake of completeness, can theoretically be used to predict the correlation width of the irradiance fluctuations and the scintillation index.

To calculate the ensemble averages appearing in Eqs. (26)–(28), we once again use the relation (Section 6.2.2)

$$\langle\exp(\psi)\rangle = \exp\left[\langle\psi\rangle + \frac{1}{2}(\langle\psi^2\rangle - \langle\psi\rangle^2)\right], \quad (29)$$

which leads to

$$\langle\exp[\psi(\mathbf{r}, \mathbf{s})]\rangle = \exp[E_1(0, 0; 0, 0)], \quad (30)$$

$$\langle\exp[\psi(\mathbf{r}_1, \mathbf{s}_1)+\psi^*(\mathbf{r}_2, \mathbf{s}_2)]\rangle = \exp[2E_1(0, 0; 0, 0)+E_2(\mathbf{r}_1, \mathbf{r}_2; \mathbf{s}_1, \mathbf{s}_2)], \quad (31)$$

and

$$\langle \exp[\psi(\mathbf{r}_1, \mathbf{s}_1) + \psi^*(\mathbf{r}_2, \mathbf{s}_2) + \psi(\mathbf{r}_3, \mathbf{s}_3) + \psi^*(\mathbf{r}_4, \mathbf{s}_4)] \rangle$$
$$= \exp\Big[4E_1(0,0;0,0) + E_2(\mathbf{r}_1, \mathbf{r}_2; \mathbf{s}_1, \mathbf{s}_2) + E_2(\mathbf{r}_1, \mathbf{r}_4; \mathbf{s}_1, \mathbf{s}_4) + E_2(\mathbf{r}_3, \mathbf{r}_2; \mathbf{s}_3, \mathbf{s}_2)$$
$$+ E_2(\mathbf{r}_3, \mathbf{r}_4; \mathbf{s}_3, \mathbf{s}_4) + E_3(\mathbf{r}_1, \mathbf{r}_3; \mathbf{s}_1, \mathbf{s}_3) + E_3^*(\mathbf{r}_2, \mathbf{r}_4; \mathbf{s}_2, \mathbf{s}_4) \Big]. \tag{32}$$

In particular, because $\langle \exp[\psi(\mathbf{r}, \mathbf{s})] \rangle = \exp[E_1(0,0;0,0)]$ is independent of $\mathbf{r}$ and $\mathbf{s}$, it becomes simply a multiplicative factor in Eq. (26), and we deduce that the *mean field* becomes

$$\begin{aligned} \langle U(\mathbf{r}, L) \rangle &= U_0(\mathbf{r}, L) \exp[E_1(0,0;0,0)] \\ &= U_0(\mathbf{r}, L) \exp\Big[-2\pi^2 k^2 L \int_0^\infty \kappa \Phi_n(\kappa)\, d\kappa \Big], \end{aligned} \tag{33}$$

where $U_0(\mathbf{r}, L)$ is the optical field in the absence of turbulence. We recognize Eq. (33) as the same result obtained in Section 6.2.3 using the Rytov method and in Section 7.2.1 using the parabolic equation method.

7.3.2 Gaussian-beam parameters

The general expressions defined by Eqs. (27) and (28) are valid for any type optical wave. As before, if we wish to consider the case of a Gaussian-beam wave with spot radius W_0 and phase front radius of curvature F_0, it is useful to characterize such a beam by the input plane beam parameters (Section 4.4.1)

$$\Theta_0 = 1 - \frac{L}{F_0}, \qquad \Lambda_0 = \frac{2L}{kW_0^2}, \tag{34}$$

where k is the optical wave number and L is the path length. At the receiver the beam is described by the similar set of beam parameters

$$\begin{aligned} \Theta &= 1 + \frac{L}{F} = \frac{\Theta_0}{\Theta_0^2 + \Lambda_0^2}, \\ \overline{\Theta} &= 1 - \Theta, \\ \Lambda &= \frac{2L}{kW^2} = \frac{\Lambda_0}{\Theta_0^2 + \Lambda_0^2}, \end{aligned} \tag{35}$$

where W and F are the beam spot radius and phase front radius of curvature, respectively, in the plane of the receiver. The limiting characteristics of a plane wave are obtained by setting $\Theta = 1$ and $\Lambda = 0$, whereas those for a spherical wave correspond to $\Theta = \Lambda = 0$.

7.3.3 Mean irradiance and beam spread

A general expression for the MCF is given by Eq. (27). The *mean irradiance* is obtained from the MCF by setting $\mathbf{r}_1 = \mathbf{r}_2 = \mathbf{r}$. For equal observation points, we see that Eq. (31) yields the relation

$$\langle \exp[\psi(\mathbf{r}, \mathbf{s}_1) + \psi^*(\mathbf{r}, \mathbf{s}_2)] \rangle = \exp\left\{ -4\pi^2 k^2 L \int_0^1 \int_0^\infty \kappa \Phi_n(\kappa)[1 - J_0(Q\kappa\xi)] d\kappa \, d\xi \right\}$$
$$= \exp\left[-\frac{1}{2} D_{\text{sp}}(Q) \right], \tag{36}$$

where $D_{\text{sp}}(Q)$ is the spherical wave structure function (WSF) (Section 6.4.2). From this result and the change of vector variables

$$\mathbf{S} = \frac{1}{2}(\mathbf{s}_1 + \mathbf{s}_2),$$
$$\mathbf{Q} = \mathbf{s}_1 - \mathbf{s}_2,$$

the MCF (27) with $\mathbf{r}_1 = \mathbf{r}_2 = \mathbf{r}$ leads to

$$\langle I(\mathbf{r}, L) \rangle = \Gamma_2(\mathbf{r}, \mathbf{r}, L)$$
$$= \left(\frac{k}{2\pi L} \right)^2 \int\int\int\int_{-\infty}^{\infty} d^2S d^2Q \exp\left(-\frac{2S^2}{W_0^2} - \frac{Q^2}{2W_0^2} \right)$$
$$\times \exp\left[\frac{ik}{L} \left(1 - \frac{L}{F_0} \right) \mathbf{S} \cdot \mathbf{Q} - \frac{ik}{L} \mathbf{r} \cdot \mathbf{Q} \right] \exp\left[-\frac{1}{2} D_{\text{sp}}(Q) \right]. \tag{37}$$

In arriving at (37), we have assumed the optical wave at the transmitter is a unit-amplitude Gaussian beam with characteristics described by Eqs. (34). By converting pairs of integrals in (37) to polar coordinates and performing three of the above integrations, we are left with the simpler result (see Prob. 4)

$$\langle I(\mathbf{r}, L) \rangle = \frac{k^2 W_0^2}{4L^2} \int_0^\infty Q J_0\left(\frac{krQ}{L} \right) \exp\left(-\frac{kQ^2}{4\Lambda L} \right) \exp\left[-\frac{1}{2} D_{\text{sp}}(Q) \right] dQ. \tag{38}$$

The quantity $z_i \sim (C_n^2 k^2 l_0^{5/3})^{-1}$ represents the propagation distance at which the transverse coherence radius of the optical wave is on the order of the inner scale l_0. Ignoring outer scale effects, assuming the propagation distance satisfies $L \gg z_i$, and assuming $q\Lambda \gg 1$, the spherical WSF can be approximated by (Section 6.4.2)

$$D_{\text{sp}}(Q) = 1.093 \, C_n^2 k^2 L l_0^{-1/3} Q^2, \quad L \gg z_i. \tag{39}$$

Under this condition, the mean irradiance (38) reduces exactly to the Gaussian function

$$\langle I(\mathbf{r}, L) \rangle = \frac{W_0^2}{W_{\text{LT}}^2} \exp\left(-\frac{2r^2}{W_{\text{LT}}^2} \right), \tag{40}$$

where W_{LT} is the *effective* or *long-term spot radius* defined by (see Prob. 5)

$$\begin{aligned} W_{\mathrm{LT}} &= W\sqrt{1 + 0.982\sigma_R^2 \Lambda Q_m^{1/6}} \\ &= W\sqrt{1 + 4q\Lambda/3}, \quad L \gg z_i. \end{aligned} \tag{41}$$

Because the WSF (39) is based on the Tatarskii spectrum [Eq. (19) in Chap. 3], it follows that $Q_m = L\kappa_m^2/k = 35.05L/kl_0^2$ and $q = 0.74\sigma_R^2 Q_m^{1/6}$. It is interesting to note that Eq. (41) can also be deduced from Eq. (47) in Chap. 6 (using the Rytov method) by assuming $\Lambda Q_m \ll 1$ and $Q_0 = L\kappa_0^2/k = 0$.[1]

In most practical situations the propagation path length satisfies $L \ll z_i$ for which

$$D_{\mathrm{sp}}(Q) \cong 1.093\, C_n^2 k^2 L Q^{5/3}, \quad L \ll z_i, \tag{42}$$

where we have ignored both inner scale and outer scale effects. The substitution of (42) into (38), followed by a change of variables, subsequently leads to

$$\langle I(\mathbf{r}, L)\rangle = \frac{2W_0^2}{W^2}\int_0^\infty t J_0\left(\frac{2\sqrt{2}rt}{W}\right)\exp(-t^2 - yt^{5/3})\, dt, \tag{43}$$

where

$$y = \frac{1}{2}D_{\mathrm{sp}}\left(2\sqrt{L\Lambda/k}\right) = 1.41\sigma_R^2\Lambda^{5/6}. \tag{44}$$

For $y \gg 1$, Eq. (43) can be approximated once again by the Gaussian function (40) where this time the effective spot size is [13,14]

$$\begin{aligned} W_{\mathrm{LT}} &\cong W\sqrt{1 + 1.63\sigma_R^{12/5}\Lambda} \\ &= W\sqrt{1 + 4q\Lambda/3}, \quad L \ll z_i, \end{aligned} \tag{45}$$

and $q = 1.22\sigma_R^{12/5}$. Although derived using strong fluctuation theory (i.e., $\sigma_R^2\Lambda^{5/6} \gg 1$), Eq. (45) for the effective spot size is also sufficiently accurate in weak fluctuation regimes that it can generally be used to predict the effective spot size under nearly all conditions of atmospheric turbulence.

[1]This is true because the form of the WSF (39) is also appropriate over very short propagation paths for which $\Lambda Q_m \ll 1$.

7.3.4 Mutual coherence function

Based on the result of Eq. (31), it follows that

$$\begin{aligned}\langle \exp[\psi(\mathbf{r}_1,\mathbf{s}_1)+\psi^*(\mathbf{r}_2,\mathbf{s}_2)]\rangle &= \exp\Big[\!\Big[-4\pi^2k^2L\int_0^1\int_0^\infty \kappa\Phi_n(\kappa) \\ &\quad\times\big\{1-J_0[|(1-\xi)\mathbf{p}+\xi\mathbf{Q}|\kappa]\big\}d\kappa\,d\xi\Big]\!\Big] \\ &= \exp\left[-\frac{1}{2}D_{\rm sp}(\mathbf{p},\mathbf{Q})\right],\end{aligned} \tag{46}$$

where $D_{\rm sp}(\mathbf{p},\mathbf{Q})$ is called the *two-point* spherical WSF. The substitution of (46) into (27) and change of vector variables

$$\begin{aligned}\mathbf{S} &= \frac{1}{2}(\mathbf{s}_1+\mathbf{s}_2),\\ \mathbf{Q} &= \mathbf{s}_1-\mathbf{s}_2 = \mathbf{p}-\left(\frac{L}{k}\right)\mathbf{u},\end{aligned}$$

ultimately leads to the expression [2,15,16]

$$\begin{aligned}\Gamma_2(\mathbf{p},\mathbf{r},L) &= \frac{W_0^2}{8\pi}\int\int_{-\infty}^{\infty} d^2u \\ &\quad\times\exp\left\{-\frac{\rho^2}{2W_B^2}-\frac{1}{8}W^2u^2+\frac{\overline{\Theta}}{2\Lambda}\mathbf{u}\cdot\mathbf{p}+i\mathbf{u}\cdot\mathbf{r}-\frac{1}{2}D_{\rm sp}\left[\mathbf{p},\mathbf{p}-\left(\frac{L}{k}\right)\mathbf{u}\right]\right\},\end{aligned} \tag{47}$$

where $\rho=|\mathbf{p}|, \mathbf{r}=\frac{1}{2}(\mathbf{r}_1+\mathbf{r}_2)$, and W_B is the beam radius at the waist (Section 4.5.1)

$$W_B = \frac{W_0|\Omega_f|}{\sqrt{1+\Omega_f^2}}, \qquad \Omega_f = \frac{2F_0}{kW_0^2}. \tag{48}$$

Also, the spherical WSF in (47) is defined by

$$D_{\rm sp}\left[\mathbf{p},\mathbf{p}-\left(\frac{L}{k}\right)\mathbf{u}\right] = 8\pi^2k^2L\int_0^1\int_0^\infty \kappa\Phi_n(\kappa)\left\{1-J_0\left[\kappa\left|\mathbf{p}-\left(\frac{L\xi}{k}\right)\mathbf{u}\right|\right]\right\}d\kappa\,d\xi. \tag{49}$$

As before, it is instructive to consider separately the cases $L\gg z_i$ and $L\ll z_i$ for the purpose of evaluating the integrals in (49).

For $L \gg z_i$, the evaluation of the integrals in (49) using the Tatarskii spectrum [Eq. (19) in Chap. 3] leads to

$$\begin{aligned} D_{\text{sp}}\left[\mathbf{p}, \mathbf{p} - \left(\frac{L}{k}\right)\mathbf{u}\right] &= 3.28\, C_n^2 k^2 L l_0^{-1/3} \int_0^1 \left|\mathbf{p} - \left(\frac{L\xi}{k}\right)\mathbf{u}\right|^2 d\xi \\ &= \frac{2}{\rho_{\text{pl}}^2}\left(\rho^2 - \frac{L}{k}\mathbf{u} \cdot \mathbf{p} + \frac{L^2 u^2}{3k^2}\right), \end{aligned} \tag{50}$$

where $\rho_{\text{pl}} = (1.64\, C_n^2 k^2 L l_0^{-1/3})^{-1/2}$ is the plane wave coherence radius. Based on the result of (50), the subsequent evaluation of the remaining integrals in (47) yields [16]

$$\Gamma_2(\mathbf{p}, \mathbf{r}, L) = \frac{W_0^2}{W_{\text{LT}}^2} \exp\left[-\frac{2r^2}{W_{\text{LT}}^2} - \frac{\rho^2}{\rho_0^2} + i\frac{2}{\Lambda}\left(\frac{\overline{\Theta} + 2q\Lambda}{W_{\text{LT}}^2}\right)\mathbf{r} \cdot \mathbf{p}\right], \quad L \gg z_1, \tag{51}$$

where W_{LT} is the long-term spot size given by (41) and ρ_0 is the transverse spatial coherence radius defined by

$$\rho_0^2 = \frac{(3 + 4q\Lambda)\rho_{\text{pl}}^2}{1 + \Theta + \Theta^2 + \Lambda^2 + 3\Lambda/4q + q\Lambda}. \tag{52}$$

For $q = 0.74\sigma_{\text{R}}^2 Q_m^{1/6} \gg \Lambda$, consistent with strong fluctuation theory, this last result can be simplified to [17]

$$\frac{\rho_0}{\rho_{\text{pl}}} = \sqrt{\frac{3 + 4q\Lambda}{1 + \Theta + \Theta^2 + \Lambda^2 + q\Lambda}}, \quad q \gg \Lambda. \tag{53}$$

Observe in the limit $q \to \infty$, that (53) leads to $\rho_0 = 2\rho_{\text{pl}}$ for all Gaussian beams (i.e., collimated, focused, or divergent). Also, note that by neglecting terms with $q\Lambda$, Eq. (53) reduces to the upper form in Eq. (78) in Chap. 6. Based on this last observation, it can be concluded that Eq. (53) represents a reasonable approximation to the spatial coherence radius of a Gaussian beam for all values of the strength of turbulence parameter q. Consequently, in the limiting cases of a plane wave ($\Theta = 1, \Lambda = 0$) or spherical wave ($\Theta = \Lambda = 0$), Eq. (53) reduces, respectively, to the conventional Rytov expressions $\rho_0 = \rho_{\text{pl}}$ and $\rho_0 = \sqrt{3}\rho_{\text{pl}}$.

If the propagation distance satisfies $L \ll z_i$ and $q\Lambda \gg 1$, Eq. (49) based on a Kolmogorov spectrum gives us

$$D_{\text{sp}}\left[\mathbf{p}, \mathbf{p} - \left(\frac{L}{k}\right)\mathbf{u}\right] = 2.91\, C_n^2 k^2 L \int_0^1 \left|\mathbf{p} - \left(\frac{L\xi}{k}\right)\mathbf{u}\right|^{5/3} d\xi. \tag{54}$$

The direct evaluation of this result is not known, but by imposing a *quadratic approximation* on the term in the integrand with exponent $5/3$, the resulting integral reduces as before to [2,12,14,16]

$$D_{\text{sp}}\left[\mathbf{p}, \mathbf{p} - \left(\frac{L}{k}\right)\mathbf{u}\right] = \frac{2}{\rho_{\text{pl}}^2}\left(\rho^2 - \frac{L}{k}\mathbf{u} \cdot \mathbf{p} + \frac{L^2 u^2}{3k^2}\right), \tag{55}$$

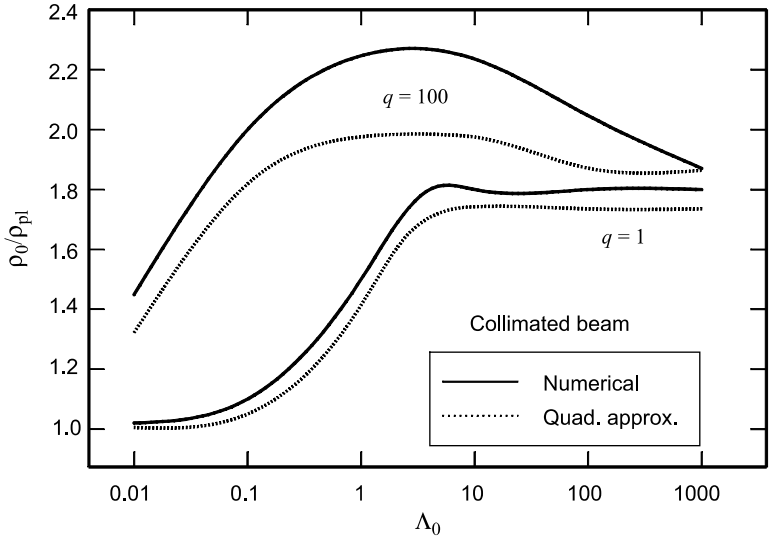

Figure 7.1 Ratio of coherence radii as a function of the Fresnel ratio Λ_0 and turbulence strengths $q = 1$ and $q = 100$. The solid curves and numerical calculations based on Eq. (47).

where $\rho_{pl} = (1.45C_n^2k^2L)^{-3/5}$ in this case. From this point, the derivation of the MCF leads once again to Eq. (60) but this time with $q = 1.22\sigma_R^{12/5}$. Thus, the implied spot size is that given by (31) and the implied spatial coherence radius is again that given by (53).

In Fig. 7.1, the coherence ratio ρ_0/ρ_{pl} deduced from Eq. (53) with $q = 1.22\sigma_R^{12/5}$ is shown (dotted curves) for a collimated beam with fixed path length as a function of Fresnel ratio Λ_0 and two values of the turbulence parameter ($q = 1$, $q = 100$). The solid curves correspond to values generated from a numerical solution of Eq. (47). In the strong turbulence case ($q = 100$) the spatial coherence radius of the beam exceeds that of a spherical wave, whereas in moderate-to-weak fluctuation regimes the corresponding coherence radius always lies between that of a plane wave and a spherical wave. Here we also see that the quadratic approximation (53) predicts the spatial coherence radius $\rho_0 = 2\rho_{pl}$ for strong turbulence ($q \to \infty$) whereas the exact numerical result is $\rho_0 = 2.27\rho_{pl}$.

The exact relation $\rho_0 = 2.27\rho_{pl}$ for a Gaussian beam in strong turbulence with $\Lambda_0 \sim 3$ was first obtained in the theoretical study of Belen'kii and Mironov [17] by using rigorous asymptotic analysis of the solution of the parabolic equation for the MCF (Section 7.2.2). In the same study, they verified this result using numerical methods.

7.4 Method of Effective Beam Parameters

Belen'kii and Mironov [18,19] found that in passing from weak to strong irradiance fluctuations the turbulence of the medium decreases the beam mean wave

front radius of curvature from that of an unbounded plane wave or spherical wave. This results in an increase in the spatial coherence radius through diffraction, which in essence defines an "effective" radius of curvature. The related notion of "effective" spot size had already been introduced many years before to characterize the average dimensions of the beam area where beam wander takes place. Although independently derived with different objectives, the effective radius of curvature and spot size are linked through simple geometric properties of Gaussian beams.

If we formally replace the zero-order Rytov approximation (i.e., the free-space field) with a "distorted Gaussian-beam wave" defined by the effective spot size and effective radius of curvature, we can then develop a pair of "effective" Gaussian beam parameters that characterize this distorted wave in the plane of the receiver. This idea is similar to that behind the distorted wave Born approximation introduced in the Russian literature in the 1970s and later reviewed by Kratsov [20]. To develop the effective beam parameters, we simply compare the free-space MCF given by [see Eq. (34) in Chap. 6]

$$\Gamma_2^0(\mathbf{p},\mathbf{r},L) = \frac{W_0^2}{W^2}\exp\left(-\frac{2r^2}{W^2} - \frac{\rho^2}{2W^2} - i\frac{k}{F}\mathbf{p}\cdot\mathbf{r}\right) \tag{56}$$

with Eq. (51) to identify the equivalent parameters. That is, by comparing the first and third arguments in the corresponding exponential functions, we first deduce that [16]

$$\begin{aligned} W \;&\Rightarrow\; W_{\mathrm{LT}} = W\sqrt{1+4q\Lambda/3}, \\ F \;&\Rightarrow\; F_{\mathrm{LT}} = -\frac{L(1+4q\Lambda/3)}{\overline{\Theta}+2q\Lambda}, \end{aligned} \tag{57}$$

which, in turn, define the pair of *effective receiver beam parameters*

$$\begin{aligned} \Theta_e &= 1+\frac{L}{F_{\mathrm{LT}}} = \frac{\Theta-2q\Lambda/3}{1+4q\Lambda/3} = \frac{\Theta-0.81\sigma_R^{12/5}\Lambda}{1+1.63\sigma_R^{12/5}\Lambda}, \\ \Lambda_e &= \frac{2L}{kW_{\mathrm{LT}}^2} = \frac{\Lambda}{1+4q\Lambda/3} = \frac{\Lambda}{1+1.63\sigma_R^{12/5}\Lambda}. \end{aligned} \tag{58}$$

Equations (58) are natural extensions of the corresponding beam parameters (35) that account for additional refraction and diffraction caused by turbulence as the beam propagates into the strong fluctuation regime. Observe that for $q \to \infty$, the limiting values are $\Theta_e = -1/2$ and $\Lambda_e = 0$. The vanishing of Λ_e suggests that the wave eventually becomes unbounded, much like a spherical wave.

7.4.1 Spatial coherence radius

The effective beam parameters (58) establish a natural link between the weak and strong fluctuation regimes. In particular, under weak fluctuation conditions, the

effective beam parameters essentially coincide with the free-space beam parameters (35). Under strong fluctuation conditions, the use of the effective beam parameters (58) allows us formally to extend weak fluctuation expressions for various second-order statistical quantities like the spatial coherence radius into the strong-fluctuation regime. For example, the formal replacement of the free-space beam parameters in Eqs. (78) in Chap. 6 with those in (58) leads directly to

$$\frac{\rho_0}{\rho_{\rm pl}} = \begin{cases} \left(\dfrac{3}{1+\Theta_e+\Theta_e^2+\Lambda_e^2}\right)^{1/2}, & \rho_0 \ll l_0, \\ \left[\dfrac{8}{3(a_e+0.62\Lambda_e^{11/6})}\right]^{3/5}, & l_0 \ll \rho_0 \ll L_0, \end{cases} \tag{59}$$

where

$$a_e = \begin{cases} \dfrac{1-\Theta_e^{8/3}}{1-\Theta_e}, & \Theta_e \geq 0, \\ \dfrac{1+|\Theta_e|^{8/3}}{1-\Theta_e}, & \Theta_e < 0. \end{cases} \tag{60}$$

The ratio of coherence radii ($\rho_0 \gg l_0$) defined by the lower expression in (59) for a collimated beam is plotted (dashed curves) in Fig. 7.2 as a function of Fresnel ratio Λ_0. For comparison, the exact numerical calculation and the quadratic approximation from Fig. 7.1 are also shown. In general, the values generated by

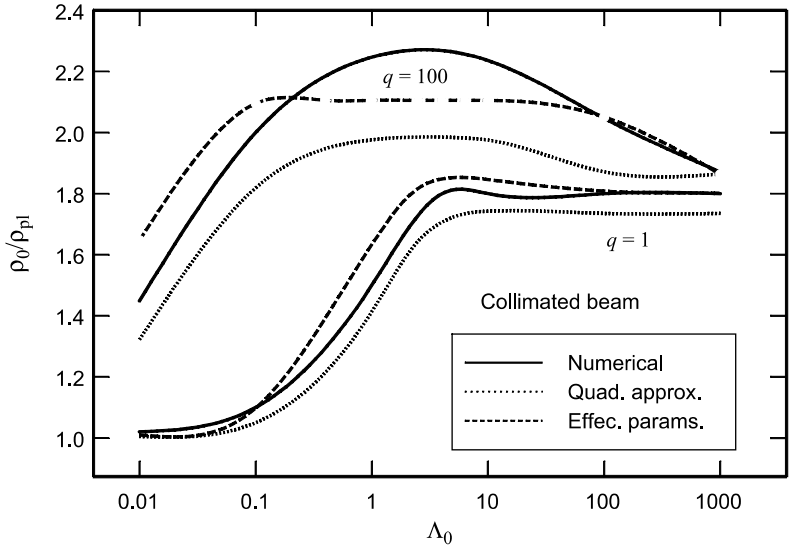

Figure 7.2 The dashed curves represent the ratio of coherence radii (59) as a function of Fresnel ratio Λ_0 and turbulence strengths $q = 1$ and $q = 100$. The solid and dotted curves are the same as those in Fig. 7.1.

(59) lie closer to the exact numerical results than those generated by Eq. (53), particularly for beams in which $\Lambda_0 > 0.1$. From Eqs. (59), the peak value of the coherence ratio for $q \to \infty$ is $\rho_0 = 2.11\rho_{\rm pl}$, which is closer to the exact value $\rho_0 = 2.27\rho_{\rm pl}$ than that predicted by Eq. (53).

For a propagating beam that is focused at distance $F_0 > 0$, the focal plane or geometric focus is defined by the Fresnel ratio at the transmitter given by (Section 4.5)

$$\Omega_f = \frac{2F_0}{kW_0^2}. \tag{61}$$

The predicted coherence ratios from Eqs. (53) and (59) for a convergent beam characterized by $\Omega_f = 1$, $W_0 = 0.5\,\text{cm}$, and $\lambda = 1.06\,\mu\text{m}$ are shown in Fig. 7.3 as a function of the Fresnel ratio Λ_0. The assumed atmospheric turbulence conditions are $C_n^2 = 10^{-14}\,\text{m}^{-2/3}, l_0 = 0$, and $L_0 = \infty$. The solid curve represents the lower expression in (59) whereas the dashed curve is from Eq. (53). For comparison, the dotted curve represents the coherence radius based on weak fluctuation theory [i.e., Eqs. (78) in Chap. 6]. Weak fluctuation theory begins to significantly deviate from the other theories for normalized distance $\Lambda_0 > 3$, corresponding to the onset of strong turbulence conditions.

In Fig. 7.4 the coherence radius scaled by the first Fresnel zone $(k\rho_0^2/L)^{1/2}$ is shown as a function of the Rytov variance σ_R^2. The coherence radius is obtained from the lower expression in (59) for various beam types. For $\sigma_R^2 < 1$, the predicted coherence radius of the spherical wave is greatest. However, as the

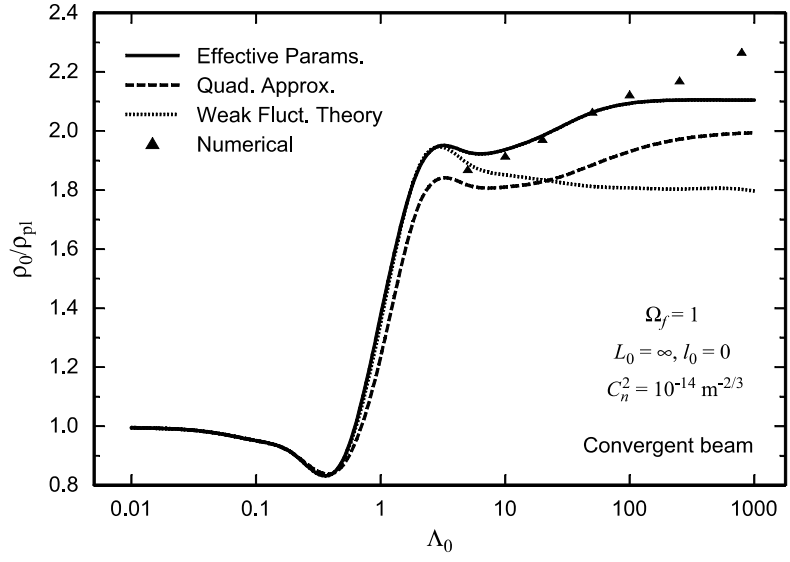

Figure 7.3 Ratio of coherence radii (59) (solid curve), (53) (dashed curve), and weak fluctuation theory (dotted curve) for a propagating beam that is initially convergent. Numerical calculations based on Eq. (47) are denoted by the field triangles. The assumed beam conditions at the transmitter are $W_0 = 1\,\text{cm}$, $\Omega_f = 1$, and $\lambda = 1.06\,\mu\text{m}$.

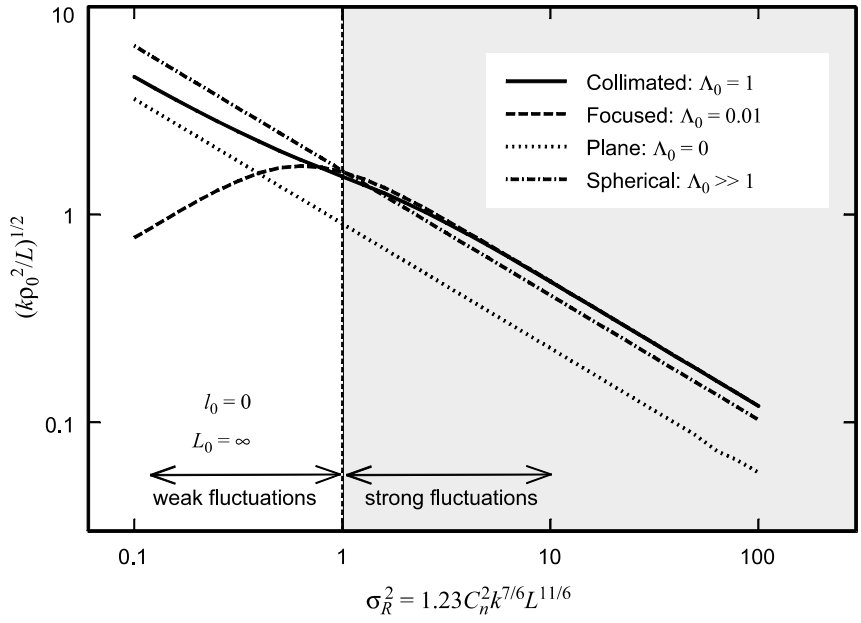

Figure 7.4 Comparison of normalized coherence radius as a function of the Rytov variance σ_R^2 for a collimated beam, a focused beam, an unbounded plane wave, and a spherical wave.

Rytov variance increases ($\sigma_R^2 \gg 1$), the coherence radii of the collimated and focused beams coincide and lie slightly above that of the spherical wave (this was previously pointed out in Refs. [17] and [18]). The coherence radius of a plane wave in strong turbulence is always less than that of other beam types.

7.4.2 Beam wander

In Section 6.6 we developed several models for the beam wander variance associated with the movement of the instantaneous center of the beam. Each of these models is dependent on beam characteristics (collimated or focused) and on whether the outer scale is taken into account or not. To generalize these expressions so they are applicable also in moderate-to-strong irradiance fluctuations, we once again resort to the effective beam parameters.

We begin with Eq. (91) in Chap. 6 for the filter function, which we now write as

$$\begin{aligned} H_{\mathrm{LS}}(\kappa, z) &= \exp\left[-\kappa^2 W_{\mathrm{LT}}^2(z)\right] \\ &= \exp\left\{-\kappa^2 W^2(z)\left[1 + 1.63\sigma_R^{12/5}(z)\Lambda(z)\right]\right\} \\ &\cong \exp\left\{-\kappa^2 W_0^2\left[(1 - z/F_0)^2 + 1.63\sigma_R^{12/5}(L)\Lambda_0(L)(z/L)^{16/5}\right]\right\}. \end{aligned} \tag{62}$$

In this equation we have simply replaced the free-space spot radius W with the effective or long-term spot radius W_{LT} and simplified the resulting expression using the geometrical optics approximation. By substituting (62) above into (90) in Chap. 6 and following the approach that led to (93) in Chap. 6, we arrive at

$$\begin{aligned}\langle r_c^2\rangle &= 1.30\,C_n^2 k L^2 W^2 \Lambda \int_0^1 \xi^2 \int_0^\infty \kappa^{-2/3}\left[1-\exp\left(-\frac{\kappa^2}{\kappa_0^2}\right)\right] \\ &\quad\times \exp\left\{-\kappa^2 W_0^2\left[\left(\Theta_0+\overline{\Theta}_0\xi\right)^2+1.63\sigma_R^{12/5}\Lambda_0(1-\xi)^{16/5}\right]\right\} d\kappa\, d\xi \\ &= 7.25 C_n^2 L^3 W_0^{-1/3}\int_0^1 \xi^2 \left[\left[\frac{1}{\left[\left(\Theta_0+\overline{\Theta}_0\xi\right)^2+1.63\sigma_R^{12/5}\Lambda_0(1-\xi)^{16/5}\right]^{1/6}}\right.\right. \\ &\quad\left.\left.-\frac{(\kappa_0 W_0)^{1/3}}{\left\{1+\kappa_0^2 W_0^2\left[\left(\Theta_0+\overline{\Theta}_0\xi\right)^2+1.63\sigma_R^{12/5}\Lambda_0(1-\xi)^{16/5}\right]\right\}^{1/6}}\right] d\xi.\end{aligned} \tag{63}$$

Equation (63) is our general result for all irradiance fluctuation conditions. Note that the beam wander variance (63) tends to zero under strong irradiance fluctuations and, under near-field weak irradiance fluctuations ($\sigma_R^2 \ll 1$), it reduces to Eq. (93) in Chap. 6.

Klyatskin and Kon [21] developed an expression for the total beam wander variance that is valid under weak and strong irradiance fluctuations. Mironov and Nosov [22] developed separate asymptotic relations for the beam wander variance that are applicable in either weak or strong irradiance-fluctuation regimes. Mironov and Nosov compared their asymptotic formulas with various experimental data for a focused beam that had been previously published several years earlier in the Russian literature. Data from Figs. 2 and 3 in Ref. [22] are replotted below in Figs. 7.5 and 7.6, respectively, for comparison with the above theoretical result. Because the experimental data was based on various focused beams, we plot the root-mean-square (rms) angular displacement $\alpha_c = \sqrt{\langle r_c^2\rangle}/L^2$ deduced from Eq. (63) for a focused beam ($\Theta_0 = 0, \overline{\Theta}_0 = 1$) versus the square root of the structure function $D_S(\sqrt{2}W_0) = 1.09 C_n^2 k^2 L\left(\sqrt{2}W_0\right)^{5/3}$. We used outer scale parameter $\kappa_0 = 1.92$ in Fig. 7.5 (based on the scaled reciprocal of laser beam height 1.3 m above ground in the experiment) and $\kappa_0 = 1.43$ in Fig. 7.6 (also equal to the scaled reciprocal of laser beam height 1.75 m above ground in the experiment). The wavelength in both cases is $\lambda = 0.63\,\mu$m, the beam radius is 10.6 cm in Fig. 7.5 and 21.35 cm in Fig. 7.6, the path length is $L = 1750$ m in both figures, and the refractive-index structure parameter was allowed to vary. Here we see that the above theoretical model (63) produces a good fit with the experimental data in both cases. Although we don't show it, the model also compares well with data shown in other figures provided in Ref. [22].

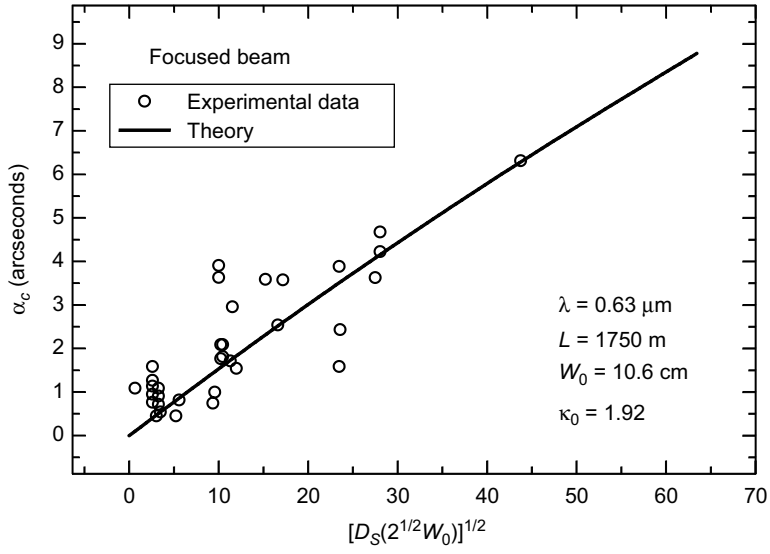

Figure 7.5 Theoretical curve and experimental data for the rms angular beam wander displacement $\alpha_c = \sqrt{\langle r_c^2 \rangle / L^2}$ versus the square root of the structure function $D_s(\sqrt{2}W_0) = 1.09 C_n^2 k^2 L (\sqrt{2}W_0)^{5/3}$.

7.5 Summary and Discussion

Up to the present chapter, we have discussed primarily weak fluctuation theory for which the *Rytov approximation* can be applied. For the Kolmogorov spectrum,

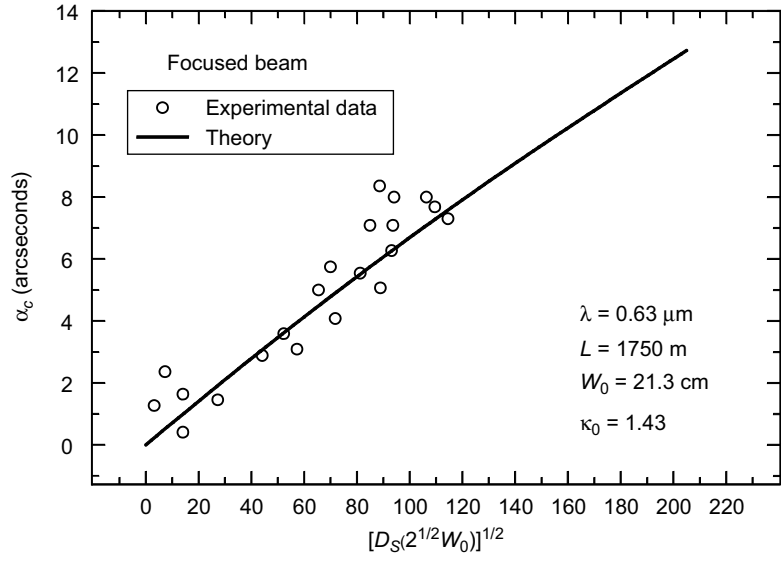

Figure 7.6 Same as Fig. 7.5 for a different set of data.

weak fluctuation theory is valid provided that $\sigma_R^2 < 1$ and $\sigma_R^2 \Lambda^{5/6} < 1$. When either of these inequalities is reversed, the fluctuations of the optical wave are considered strong. Weak fluctuation theory applied under strong fluctuation conditions can lead to erroneous results. Among others, it leads to the following inaccuracies:

- *underestimation* of the effective spot size of the beam wave
- *underestimation* of the spatial coherence radius of the beam wave
- *overestimation* of the scintillation index

Several approaches have been proposed for dealing with propagation problems involving strong irradiance fluctuations. Up through second moments of the optical field, these various methods generally lead to the same results under certain assumptions. The *extended Huygens-Fresnel principle* (Section 7.3) often provides the simplest formulation for strong fluctuation regimes, but it has not been established that it produces the same results for the fourth-order moment as other theories, such as the parabolic equation method. Exact solutions for the fourth-order field moment have thus far not been obtained by any method.

The solution for the first-order field moment, or *mean field*, is given by

$$\langle U(\mathbf{r}, L)\rangle = U_0(\mathbf{r}, L) \exp\left(-0.39 C_n^2 k^2 L \kappa_0^{-5/3}\right), \tag{64}$$

where the von Kármán spectrum has been used and $\kappa_0 \sim 1/L_0$. This same result is predicted by virtually all methods, including the Rytov approximation. In addition, for the special cases of a plane wave or spherical wave, the second-order field moment, or *mutual coherence function* (MCF), predicted by strong fluctuation theories is also the same as that predicted by the Rytov method, viz.,

$$\Gamma_2(\mathbf{p}, \mathbf{r}, L) = \begin{cases} \exp\left[-\dfrac{1}{2} D(\rho, L)\right], & (\text{plane wave}), \\ \dfrac{1}{(4\pi L)^2} \exp\left[\dfrac{ik}{L}\mathbf{p} \cdot \mathbf{r} - \dfrac{1}{2} D(\rho, L)\right], & (\text{spherical wave}), \end{cases} \tag{65}$$

where $D(\rho, L)$ is the WSF defined for a plane wave and spherical wave, respectively, by Eqs. (62) and (69) in Chap. 6. However, distinctions in the MCF arise between strong fluctuation results and weak fluctuation results for the case of a Gaussian-beam wave. Although exact only for $L \gg z_i$, strong fluctuation theory predicts that the MCF can be approximated under all conditions by

$$\Gamma_2(\mathbf{p}, \mathbf{r}, L) = \frac{W_0^2}{W_{\mathrm{LT}}^2} \exp\left(-\frac{2r^2}{W_{\mathrm{LT}}^2} - \frac{\rho^2}{\rho_0^2} - \frac{ik}{F_{\mathrm{LT}}}\mathbf{r} \cdot \mathbf{p}\right), \tag{66}$$

where W_{LT} and F_{LT} are the long-term or effective spot size and phase front radius of curvature of the Gaussian beam described by

$$\begin{aligned} W_{\mathrm{LT}} &= W\sqrt{1 + 4q\Lambda/3}, \\ F_{\mathrm{LT}} &= -\frac{L(1 + 4q\Lambda/3)}{\overline{\Theta} + 2q\Lambda}, \end{aligned} \tag{67}$$

and where

$$q = \frac{L}{k\rho_{\mathrm{pl}}^2} = \begin{cases} 1.22(\sigma_R^2)^{6/5}, & \rho_{\mathrm{pl}} \gg l_0 \\ 1.33\sigma_R^2\left(\dfrac{L}{kl_0^2}\right)^{1/6}, & \rho_{\mathrm{pl}} \ll l_0. \end{cases} \tag{68}$$

In the above results, W_0 and W are the diffractive spot radii at the transmitter and receiver, Θ and Λ are Gaussian beam parameters defined by Eqs. (17), ρ_0 is the spatial coherence radius of a Gaussian-beam wave, and ρ_{pl} is the spatial coherence radius of a plane wave.

The *spatial coherence radius* appearing in (66) is defined by

$$\frac{\rho_0}{\rho_{\mathrm{pl}}} = \sqrt{\frac{3 + 4q\Lambda}{1 + \Theta + \Theta^2 + \Lambda^2 + q\Lambda}}, \quad q \gg \Lambda. \tag{69}$$

Perhaps of particular interest is that the spatial coherence radius of a collimated beam can exceed that of a spherical wave in strong fluctuation regimes, whereas the predicted coherence radius under weak fluctuation conditions always lies between that of a plane wave and a spherical wave. In addition, the mean irradiance for a focused beam in strong fluctuation conditions soon approaches that of a collimated beam; moreover, the ability to focus a beam disappears altogether as the turbulence strength increases.

An alternate expression for the spatial coherence radius (66) has been derived by using the technique of *effective beam parameters*, which leads to

$$\frac{\rho_0}{\rho_{\mathrm{pl}}} = \begin{cases} \left|\dfrac{3}{1 + \Theta_e + \Theta_e^2 + \Lambda_e^2}\right|^{1/2}, & \rho_0 \ll l_0, \\ \left[\dfrac{8}{3(a_e + 0.62\Lambda_e^{11/6})}\right]^{3/5}, & l_0 \ll \rho_0 \ll L_0. \end{cases} \tag{70}$$

The effective beam parameters appearing in (70) are defined by

$$\Theta_e = 1 + \frac{L}{F_{\mathrm{LT}}} = \frac{\Theta - 2q\Lambda/3}{1 + 4q\Lambda/3}, \qquad \Lambda_e = \frac{2L}{kW_{\mathrm{LT}}^2} = \frac{\Lambda}{1 + 4q\Lambda/3}, \tag{71}$$

$$a_e = \begin{cases} \dfrac{1 - \Theta_e^{8/3}}{1 - \Theta_e}, & \Theta_e \geq 0, \\ \dfrac{1 + |\Theta_e|^{8/3}}{1 - \Theta_e}, & \Theta_e < 0. \end{cases} \tag{72}$$

Under weak irradiance fluctuations, beam wander can be quite prominent for certain types of beams, but under strong fluctuations the effect of beam wander tends to subside because the beam breaks up into several smaller pieces. Using the effective beam parameters (actually, the effective or long-term beam radius W_{LT}) the *variance of beam wander* is given by

$$\langle r_c^2 \rangle = 7.25 C_n^2 L^3 W_0^{-1/3} \int_0^1 \xi^2 \left[\left[\frac{1}{\left[\left(\Theta_0 + \overline{\Theta}_0 \xi \right)^2 + 1.63 \sigma_R^{12/5} \Lambda_0 (1 - \xi)^{16/5} \right]^{1/6}} \right. \right.$$
$$\left. \left. - \frac{(\kappa_0 W_0)^{1/3}}{\left\{ 1 + \kappa_0^2 W_0^2 \left[\left(\Theta_0 + \overline{\Theta}_0 \xi \right)^2 + 1.63 \sigma_R^{12/5} \Lambda_0 (1 - \xi)^{16/5} \right] \right\}^{1/6}} \right] \right] d\xi. \tag{73}$$

Unlike our weak irradiance fluctuation expression developed in Chap. 6, here there is little simplification that results by separately considering a collimated beam or a focused beam. And, although we can reduce the integral in (73) to a simpler algebraic function in the limiting case of infinite outer scale (i.e., $\kappa_0 \to 0$), once again it is difficult to evaluate the integral in a simple analytic form.

7.6 Worked Examples

Example 1: For the case of a collimated beam propagating under either very weak turbulence conditions ($q \ll \Lambda$) or very strong turbulence ($q \gg \Lambda$), where $q = L/k\rho_{\mathrm{pl}}^2$, show that Eq. (52) can be reduced to

$$\rho_0 \cong \sqrt{2} W, \quad q \ll \Lambda,$$
$$\rho_0 \cong 2\rho_{\mathrm{pl}}, \quad q \gg \Lambda.$$

Solution: For the case $q \ll \Lambda$, Eq. (52) can be expressed as

$$\frac{\rho_0^2}{\rho_{\rm pl}^2} \cong \frac{4q}{\Lambda} = \frac{4L}{k\rho_{\rm pl}^2\Lambda} = \frac{2W^2}{\rho_{\rm pl}^2},$$

which reduces to the expression given above, $\rho_0 = \sqrt{2}W$. Basically, this relation shows that the spatial coherence radius coincides with the diffractive radius of the beam under sufficiently weak fluctuation conditions.

But, when $q \gg \Lambda$, Eq. (52) takes the form

$$\frac{\rho_0^2}{\rho_{\rm pl}^2} \cong \frac{4q\Lambda}{q\Lambda} = 4,$$

which produces the second expression above, $\rho_0 = 2\rho_{\rm pl}$. This expression reveals that the spatial coherence radius of a beam wave in sufficiently strong fluctuations exceeds the spatial coherence of a spherical wave given by $\rho_{\rm sp} = 1.8\rho_{\rm pl}$.

❑

Problems

Section 7.2

1. Use the result of Problem 1 in Chap. 5 to show that ($\kappa_0 \sim 1/L_0$)

   (*a*) $A_n(0) - A_n(\rho) = 0.78C_n^2\kappa_0^{5/3}\left[1 - (\kappa_0\rho)^{5/6}K_{5/6}(\kappa_0\rho)\right]$.

   (*b*) Express the Bessel function in (*a*) in terms of the modified Bessel function of the first kind [see Eq. (13) in Appendix I] and use small argument approximations to deduce that the answer in part (*a*) reduces to

   $$A_n(0) - A_n(\rho) \sim C_n^2\rho^{5/3}, \quad \rho \ll L_0.$$

2. Verify that Eq. (20) is a formal solution of Eq. (18) subject to the condition (19).

Section 7.3

3. For a beam exiting the emitting aperture of a transmitter with spot radius W_0 and focused in the plane of a receiver at distance L from the source,

   (*a*) show that the effective spot radius (45) in the receiver plane takes the form

   $$W_{\mathrm{LT}} \cong \frac{2L}{kW_0}\sqrt{1 + \frac{2}{3}\left(\frac{W_0}{\rho_{\mathrm{pl}}}\right)^2},$$

   where ρ_{pl} is the coherence radius of a plane wave propagating over the same path.

   (*b*) If $\rho_{\mathrm{pl}} \ll W_0$, deduce that the effective spot radius cannot be smaller than

   $$W_{\mathrm{LT}} \cong \frac{1.63L}{k\rho_{\mathrm{pl}}}.$$

4. Given that the mean irradiance is described by

   $$\langle I(\mathbf{r}, L)\rangle = \left(\frac{k}{2\pi L}\right)^2 \int\int\int\int_{-\infty}^{\infty} d^2S d^2Q \exp\left(-\frac{2S^2}{W_0^2} - \frac{Q^2}{2W_0^2}\right) \times \exp\left[\frac{ik}{L}\left(1 - \frac{L}{F_0}\right)\mathbf{S}\cdot\mathbf{Q} - \frac{ik}{L}\mathbf{r}\cdot\mathbf{Q}\right]\exp\left[-\frac{1}{2}D_{\mathrm{sp}}(Q)\right],$$

   (*a*) make the change of variables $\mathbf{S} = (S\cos\varphi, S\sin\varphi)$ to deduce that

   $$\int\int_{-\infty}^{\infty} d^2S \exp(-2S^2/W_0^2)\exp\left(\frac{ik\Theta_0}{L}\mathbf{S}\cdot\mathbf{Q}\right) = \frac{\pi W_0^2}{2}\exp\left(-\frac{k^2W_0^2\Theta_0^2Q^2}{8L^2}\right),$$

   where $\Theta_0 = 1 - L/F_0$.

(*b*) Use the result of part (*a*) to show that the mean irradiance can be written as

$$\langle I(\mathbf{r}, L)\rangle = \frac{k^2 W_0^2}{4L^2}\int_0^\infty QJ_0\left(\frac{krQ}{L}\right)\exp\left(-\frac{kQ^2}{4\Lambda L}\right)\exp\left[-\frac{1}{2}D_{\rm sp}(Q)\right]dQ.$$

Hint: Use integrals #9 and #11 in Appendix II.

5. If the spherical WSF in Eq. (37) is given by

$$D_{\rm sp}(Q) = 1.093\, C_n^2 k^2 L l_0^{-1/3} Q^2,$$

show that the mean irradiance is given by the Gaussian function (40) with effective spot radius

$$W_{\rm LT} = W\sqrt{1 + 0.982\,\sigma_R^2 \Lambda Q_m^{1/6}}.$$

6. Given that the MCF can be expressed in the form

$$\Gamma_2(\mathbf{p}, \mathbf{r}, L) = \frac{W_0^2}{8\pi}\int\int_{-\infty}^{\infty} d^2u \exp\left\{-\frac{\rho^2}{2W_B^2} - \frac{1}{8}W^2u^2 + \frac{\overline{\Theta}}{2\Lambda}\mathbf{u}\cdot\mathbf{p} + i\mathbf{u}\cdot\mathbf{r} - \frac{1}{2}D_{\rm sp}\left[\mathbf{p}, \mathbf{p} - \left(\frac{L}{k}\right)\mathbf{u}\right]\right\},$$

where the two-point WSF is defined by

$$D_{\rm sp}[\mathbf{p}, \mathbf{p} - (L/k)\mathbf{u}] = \frac{2}{\rho_{\rm p1}^2}\left(\rho^2 - \frac{L}{k}\mathbf{u}\cdot\mathbf{p} + \frac{L^2u^2}{3k^2}\right),$$

(*a*) show that the MCF becomes

$$\Gamma_2(\mathbf{p}, \mathbf{r}, L) = \frac{W_0^2}{W_{\rm LT}^2}\exp\left[-\frac{2r^2}{W_{\rm LT}^2} - \frac{\rho^2}{\rho_0^2} + i\frac{2}{\Lambda}\left(\frac{\overline{\Theta} + 2q\Lambda}{W_{\rm LT}^2}\right)\mathbf{r}\cdot\mathbf{p}\right], \quad L \gg z_i,$$

where the spatial coherence radius ρ_0 is defined by Eq. (52).

(*b*) From the imaginary term in the exponential function in part (*a*), deduce that the effective radius of curvature is given by

$$F_{\rm LT} = -\frac{L(1 + 4q\Lambda/3)}{\overline{\Theta} + 2q\Lambda}.$$

Section 7.4

7. A collimated beam of radius 3 cm at the transmitter and of wavelength 1.55 μm is propagated 1 km through atmospheric turbulence with

$C_n^2 = 1.7 \times 10^{-14}\,\mathrm{m}^{-2/3}$. Given that the short-term beam radius W_{ST} satisfies the relation $W_{\mathrm{ST}}^2 = W_{\mathrm{LT}}^2 - \langle r_c^2 \rangle$, use the Kolmogorov spectrum to

(*a*) calculate the long-term spot radius.
(*b*) calculate the short-term beam radius.
(*c*) Solve (*a*) and (*b*) for a 5-km path.

8. If the beam in Prob. 7 has radius 1 cm, what is the beam wander variance assuming

(*a*) $C_n^2 = 1.7 \times 10^{-14}\,\mathrm{m}^{-2/3}$?
(*b*) $C_n^2 = 5 \times 10^{-13}\,\mathrm{m}^{-2/3}$?

References

1. A. M. Prokhorov, F. V. Bunkin, K. S. Gochelashvily, and V. I. Shishov, "Laser irradiance in turbulent media," *Proc. IEEE* **63**, 790–809 (1975).
2. A. Ishimaru, *Wave Propagation and Scattering in Random Media* (IEEE Press, Piscataway, NJ, 1997); [previously published as Vols I & II by Academic, New York (1978)].
3. Z. I. Feizulin and Yu. A. Kravtsov, "Expansion of a laser beam in a turbulent medium," *Izv. Vyssh, Uchebn. Zaved. Radiofiz.* **24**, 1351–1355 (1967).
4. R. F. Lutomirski and H. T. Yura, "Propagation of a finite optical beam in an inhomogeneous medium," *Appl. Opt.* **10**, 1652–1658 (1971).
5. R. Dashen, "Path integrals for waves in random media," *J. Math. Phys.* **20**, 894–920 (1979).
6. V. I. Tatarskii and V. U. Zavorotnyi, "Strong fluctuations in light propagation in a randomly inhomogeneous medium," in *Progress in Optics III*, E. Wolf, ed. (Elsevier, New York, 1980).
7. J. W. Strohbehn, "Line of sight wave propagation through the turbulent atmosphere," *Proc. IEEE* **56**, 1301–1318 (1968).
8. H. Yura, "Mutual coherence function of a finite cross section optical beam propagating in a turbulent medium," *Appl. Opt.* **11**, 1399–1406 (1972).
9. V. I. Tatarskii, *The Effects of the Turbulent Atmosphere on Wave Propagation* (trans. from the Russian and issued by the National Technical Information Office, U.S. Dept. of Commerce, Springfield, 1971).
10. K. Furutsu, "On the statistical theory of electromagnetic waves in a fluctuating medium," *J. Res. NBS* **67**D, 303–310 (1963).
11. E. A. Novikov, "Functionals and the random-force method in turbulence theory," *Sov. Phys. JETP* **20**, 1290–1294 (1965).
12. H. T. Yura and S. G. Hanson, "Second-order statistics for wave propagation through complex optical systems," *J. Opt. Soc. Am. A* **6**, 564–575 (1989).
13. W. P. Brown, Jr., "Second moment of a wave propagating in a random medium," *J. Opt. Soc. Am.* **61**, 1051–1059 (1971).
14. V. E. Zuev, *Laser Beams in the Atmosphere* (Consultants Bureau, New York, 1982), trans. by S. Wood.
15. R. L. Fante, "Electromagnetic beam propagation in turbulent media," *Proc. IEEE* **63**, 1669–1692 (1975).
16. L. C. Andrews, W. B. Miller, and J. C. Ricklin, "Spatial coherence of a Gaussian-beam wave in weak and strong optical turbulence," *J. Opt. Soc. Am. A* **11**, 1653–1660 (1994).
17. M. S. Belen'kii and V. L. Mironov, "Turbulent distortions of the spatial coherence of a laser beam," *Sov. J. Quant. Electron.* **7**, 287–290 (1977).
18. M. S. Belen'kii and V. L. Mironov, "Coherence of the field of a laser beam in a turbulent atmosphere," *Sov. J. Quant. Electron.* **10**, 595–597 (1980).
19. M. S. Belen'kii and V. L. Mironov, "Mean diffracted rays of an optical beam in a turbulent medium," *J. Opt. Soc. Am.* **70**, 159–163 (1980).

20. Yu. A. Kratsov, "Propagation of electromagnetic waves through a turbulent atmosphere," *Rep. Prog. Phys.* 39–112 (1992).
21. V. I. Klyatskin and A. I. Kon, "On the displacement of spatially bounded light beams in a turbulent medium in the Markovian-random-process approximation," *Radiofiz. Quantum Electron.* **15**, 1056–1061 (1972).
22. V. L. Mironov and V. V. Nosov, "On the theory of spatially limited light beam displacements in a randomly inhomogeneous medium," *J. Opt. Soc. Am.* **67**, 1073–1080 (1977).